Boundary-layer Features in Limit of Conservative Nonlinear Oscillators

Yair Zarmi (zarmi@bgu.ac.il)
Ben-Gurion University of the Negev - Sede Boqer Campus https://orcid.org/0000-0001-8830-9667

Research Article

Keywords: periodic saw-tooth shape, velocity, x'(t), asymptotic shapes, oscillations.

Posted Date: December 30th, 2021

DOI: https://doi.org/10.21203/rs.3.rs-1086177/v1

Boundary-layer features in limit of conservative nonlinear oscillators

Yair Zarmi
The Jacob Blaustein Institutes for Desert Research
Ben-Gurion University of the Negev
Midreshet Ben-Gurion, 8499000, Israel

Abstract

In the double limit of high amplitude ($x_{\max} \to \infty$) and high leading power (x^{2N+1}, $N \to \infty$), (1+1) dimensional conservative nonlinear oscillatory systems exhibit characteristics akin to boundary layer phenomena. The oscillating entity, $x(t)$, tends to a periodic saw-tooth shape of linear segments, the velocity, $x'(t)$, tends to a periodic step-function and the $x - x'$ phase-space plot tends to a rectangle. This is demonstrated by transforming x and t into proportionately scaled variables, η and θ, respectively. $\eta(\theta)$ is $(2\text{-}\pi)$ periodic in θ and bounded ($|\eta(\theta)| \leq 1$). The boundary-layer characteristics show up by the fact that the deviations of $\eta(\theta)$, $\eta'(\theta)$ and the $\eta - \eta'$ phase-space plot from the sharp asymptotic shapes occurs over a range in θ of $O(1/N)$ near the turning points of the oscillations.

Email: zarmi@bgu.ac.il
Orcid: 0000-0001-8830-9667

1. Introduction

There are hundreds of papers, dozens of textbooks, lecture notes and research theses that discuss the periodic behavior of linear systems, to which a small nonlinear perturbation is added, through a perturbative analysis. However, there is no satisfactory methodology for the study of such systems in the large-amplitude limit, when the nonlinear perturbation is large compared to the linear part of the equation. Absence of such methodology may be a consequence of the fact that high amplitudes go hand in hand with high acceleration. For an oscillating mass, the classical description then ceases to be valid; relativistic effects enter.

However, there are many applications in Physics (e.g., current oscillations in electronic devices), Chemistry and Biology (e.g., oscillations in chemical reactions) and Engineering (e.g., oscillations of mechanical systems), where non-relativistic large-amplitude oscillations are of relevance. The literature has focused mainly on large-amplitude oscillations of periodically driven oscillatory systems, in connection with resonance phenomena or chaotic behavior.

This paper focuses on the large-amplitude and high exponent limits of solutions of conservative systems of linear oscillators, to which nonlinear terms are added. Closed-form solutions have been derived the cases of the Duffing and Quintic oscillators [1-6]. There are works that have dealt with such systems through various expansion methods [7-35]. In all of the approximation approaches, the validity of the numerical approximations to the solution is limited in time, typically, to several periods, because the period is computed with some approximation method. To see how this problem arises, consider a nonlinearly perturbed harmonic oscillator:

$$x''(t) + x(t) + f(x(t)) = 0, \tag{1}$$

where $f(x)$ is a nonlinear function of $x(t)$. A perturbation analysis can be developed as long as

$$\left| f(x(t)) \right| \ll O\left(\left| x(t) \right| \right). \tag{2}$$

When the amplitude of oscillations, $x_{\max}$, is very large, the magnitude of $f(x)$ can be much greater than that of the linear term. Consider the following equation of motion:

$$x''(t) + x(t) + \sum_{n=1}^{2N+1} a_n x(t)^n = 0 \quad , \quad a_{2N+1} > 0. \tag{3}$$

Often, for leading nonlinear term, ($a_{2N+1}\, x^{2N+1}$), one assumes $a_{2N+1} = \varepsilon \ll 1$. However, when the maximal amplitude, $x_{\max}$ is very large, the magnitude of ε is irrelevant. What counts is the

fact that the leading term is much greater than the next-to-leading term, ($a_{2\,N-1}\,x^{2\,N-1}$). For large $x_{\max}$, the maximal velocity of oscillations, $v_{\max}$, and the period of oscillations, T, vary as:

$$v_{\max} \sim \left(x_{\max}\right)^{N+1} \quad , \quad T \sim \left(x_{\max}\right)^{-N} \quad , \quad x_{\max} \to \infty \ . \tag{4}$$

As a result, the characteristics of the solution for large $x_{\max}$ are determined by a simpler equation, which provides an approximation that improves as $x_{\max}$ grows:

$$x''\left(t\right) + a_{2N+1}\,x\left(t\right)^{2N+1} = 0 \quad , \quad N \geq 1 \quad , \quad a_{2N+1} > 0 \ . \tag{5}$$

The solutions of the full equation, Eq. (3) and of Eq. (5) will be analyzed around the (large-amplitude limit) solution by an expansion in terms of a small parameter, μ:

$$\mu = \left(a_{2N+1}\right)^{1/2N} \Big/ x_{\max} \ll 1 \ . \tag{6}$$

Using Eq. (6), the general expression for the period, T, has the form:

$$\begin{aligned} & T = \mu^N\, G \\ & G = 4\int_0^{\pi/2} \frac{1}{\left(\mu^{2N} + \sum_{n=1}^{2N+1} \mu^{2N+1-n}\, \frac{2}{\left(n+1\right)}\, \frac{a_n}{\left(a_{2N+1}\right)^{(n-1)/(2N)}}\, \frac{\left(1-\sin\left(\varphi\right)^{n+1}\right)}{\left(1-\sin\left(\varphi\right)^{2}\right)}\right)^{1/2}} d\varphi \ . \\ & \lim_{\mu\to 0} G = 4\sqrt{N+1}\int_0^{\pi/2} \frac{\cos\left(\varphi\right)}{\sqrt{\left(1-\sin\left(\varphi\right)^{2(N+1)}\right)}}\, d\varphi \equiv G_0 \end{aligned} \tag{7}$$

In the large-N limit, one has

$$G_0 \underset{N\gg 1}{\to} 4\sqrt{N}\int_0^{\pi/2} \cos\varphi\, d\varphi = 4\sqrt{N} \ . \tag{8}$$

Fig. 1 shows how G_0 of Eq. (7) approaches the large-N limit of Eq. (8). To get a difference of the order of 1%, one needs to go to rather high values of N.

We shall be interested primarily in G_0, the large-amplitude limit of G. As the discussion is limited to conservative systems, T can be computed. In the cases of N =1 and 3 (cubic and quintic oscillators, respectively), the large-amplitude limit of T has the form:

$$T_3 \to \mu\sqrt{2\pi}\,\frac{\Gamma\left(1/4\right)}{\Gamma\left(3/4\right)} \quad , \quad T_5 \to \mu^2\, 4\sqrt{3\pi}\,\frac{\Gamma\left(7/6\right)}{\Gamma\left(2/3\right)} \ . \tag{9}$$

With more complicated nonlinearities, T can be computed numerically to any desired accuracy. G_0, the leading term in G is $O(\mu^0)$. The next-to-leading term in the expression in G is determined by the next-to-leading term in Eq. (3). If that term is $a_{2q+1}\,x(t)^{2q-1}$ ($q < N$), the deviation of G from G_0 is $O(\mu^{2(N-q)})$. In the case of the simpler Eq. (5), the deviation of G from G_0 is $O(\mu^{2N})$. In the case of the cubic oscillator (Duffing), the correction is $O(\mu^2)$.

In standard expansion approaches, the period is approximated through a perturbation scheme. From Eq. (4), it is clear that $x(t)$ and $x'(t)$ vary rapidly between zero and exceedingly large values over a very short time span. A perturbation-type approximation is bound to produce results of limited validity in time. A better way to study the large-amplitude and large-N limits is based on rescaling the $x(t)$ and t:

$$x(t) = x_{\max}\,\eta(\theta) \quad , \quad \theta = (2\pi t/T) \ . \tag{10}$$

$\eta(\theta)$, is bounded ($|\eta(\theta)| \le 1$) and (2-π) periodic in θ. T is computed exactly, either in closed form, or numerically with a desired high accuracy. There is then no need to worry about the long-time quality of an approximation owing to the emergence of secular terms.

Applying Eq. (10) to Eq. (3), the equation for $\eta(\theta)$ is:

$$\eta''(\theta) + \left(\frac{T}{2\pi}\right)^2 \left\{\eta(\theta) + \sum_{n=1}^{2N+1} a_n\, x_{\max}{}^{n-1}\,\eta(\theta)^n\right\} = 0 \ . \tag{11}$$

Exploiting the asymptotic behavior of T (Eq. (4)), as $x_{\max} \to \infty$, Eq. (11) tends to the equation for η_0, the solution in the limit $x_{\max} \to \infty$:

$$\eta_0''(\theta) + \left(G_0/(2\pi)\right)^2 \eta_0(\theta)^{2N+1} = 0 \ . \tag{12}$$

η_0 for the Duffing Equation is presented in Section 2. The characteristics of the solution of Eq. (12) for $N \ge 1$ are discussed in Section 3. It is shown that, as N grows, $\eta_0(\theta)$, $\eta_0'(\theta)$ and the η_0 - η_0' phase-space plot approach periodic shapes of, respectively, a saw-tooth of linear segments, a step function and a rectangle. For large but finite N, $\eta_0(\theta)$ exhibits the characteristics of a boundary-layer system: The deviation of the actual plots of $\eta_0(\theta)$ and $\eta_0'(\theta)$ around the turning points from the sharp, $N \to \infty$, shapes occurs over a range in θ that is $O(1/N)$. Finally, for large but finite $x_{\max}$, η_0 provides an excellent approximation to the solution of Eq. (11). This is studied in Section 4.

2. The Duffing equation

The solution of the Duffing equation,

$$x''(t) + x(t) + \varepsilon x(t)^3 = 0 \quad , \quad \varepsilon > 0 \ . \tag{13}$$

is known in closed form [1-6]. Its analysis in the formulation offered here is performed as a simple example for the procedure.

The total energy is given by:

$$E = \frac{1}{2}x(t)^2 + \frac{1}{2}x'[t]^2 + \frac{1}{4}\varepsilon x[t]^4 = \frac{1}{2}{x_{\max}}^2 + \frac{1}{4}\varepsilon {x_{\max}}^4 \ . \tag{14}$$

Solving Eq. (13) for $x'(t)$, one obtains

$$x'(t) = \pm\sqrt{2}\sqrt{E - \frac{1}{2}x(t)^2 - \frac{1}{4}\varepsilon x(t)^4} \ . \tag{15}$$

Eq. (15) yields the expression for the period of oscillations:

$$T = \frac{4}{\sqrt{1+\varepsilon {x_{\max}}^2}} K\left(\sqrt{\frac{\varepsilon {x_{\max}}^2}{2\left(1+\varepsilon {x_{\max}}^2\right)}}\right) = \frac{4\mu}{\sqrt{1+\mu^2}} K\left(\frac{1}{\sqrt{2\left(1+\mu^2\right)}}\right), \tag{16}$$

where μ is defined in Eq. (6) and $K(k)$ is the complete elliptic integral of the second type [36],

$$K(k) = \int_0^{\pi/2} \left(1\Big/\sqrt{1-k^2\sin\varphi^2}\right) d\varphi \ . \tag{17}$$

Note that the relative deviation of T from the large-amplitude limit ($\mu \to 0$) is $O(\mu^2)$, which is nothing but the order of magnitude of the maximal ratio of the linear term to the cubic term in Eq. (13). As $x_{\max}$ becomes large, one has

$$\begin{aligned} v_{\max} = \max\left|x'(t)\right| = \sqrt{\frac{\varepsilon}{2}}{x_{\max}}^2 = \left(\frac{1}{\sqrt{2\varepsilon}}\right)\Big/\mu^2 \\ T \to \sqrt{\frac{2\pi}{\varepsilon}}\frac{\Gamma(1/4)}{\Gamma(3/4)}\Big/x_{\max} = 5.24412\,\mu \end{aligned} \ . \tag{18}$$

Thus, the maximal amplitude and velocity grow while the period decreases.

Using Eq. (10), Eq. (13) is transformed into:

$$\eta''(\theta) + \frac{T^2}{4\pi^2}\eta(\theta) + \frac{{x_{\max}}^2 T^2 \varepsilon}{4\pi^2}\eta(\theta)^3 = 0 \ . \tag{19}$$

In the limit of $x_{max} \to \infty$, Eq. (19) tends to:

$$\eta_0''(\theta) + \frac{\Gamma(1/4)^2}{2\pi\Gamma(3/4)^2}\eta_0(\theta)^3 = \eta_0''(\theta) + 1.3932\,\eta_0(\theta)^3 = 0\ . \tag{20}$$

For the initial conditions $\eta_0(0) = 1$, $\eta_0'(0) = 0$, the solution of Eq. (20) is:

$$\eta_0(\theta) = sn\left(\frac{\Gamma(1/4)}{4\sqrt{\pi}\Gamma(3/4)}(\pi + 2\theta), -1\right) = sn\left(1.31103 + 0.834627\theta, -1\right)\ , \tag{21}$$

where *sn* is a Jacobi elliptic function [36]. $\eta_0(\theta)$ varies in the range ±1 and $\eta_0'(0)$ - in the range $\pm 1/(2\sqrt{\pi})\ \Gamma(1/4)/\Gamma(3/4) = \pm 0.834627$.

Writing the solution as a Fourier series,

$$\eta_0(\theta) = \sum_{n=1}^{\infty} a_{2n+1}\sin\left((2n+1)\theta\right)\ , \tag{22}$$

the spectrum is dominated by the first two Fourier components: $a_1 = 0.9550$ and $a_3 = -0.0430$. The next Fourier coefficient a_5 is already 0.0019.

3. The limits of x_{max} and $N \to \infty$

3.1 The maximum of $\eta_0'(\theta)$

Eq. (12) determines $\eta_0(\theta)$, the limit of $\eta(\theta)$ as $x_{max} \to \infty$. The solution for Eq. (12) in the cases $N = 1$ and 2 are known [1-6]. In general, for $N > 1$, closed form expressions are not available.

From the energy conservation relation for Eq. (12), one calculates the maximal value of $\eta_0'(\theta)$:

$$v_{max} = \max\left(\left|\eta_0'(\theta)\right|\right) = \frac{G_0}{2\pi\sqrt{N+1}}\ . \tag{23}$$

Exploiting Eq. (16), the large-*N* limit, Eq. (23) is found to be:

$$v_{max} \underset{N\to\infty}{\to} \frac{2}{\pi}\ . \tag{24}$$

3.2 Boundary-layer characteristics of $\eta_0(\theta)$

Exploiting Eq. (10), Eq. (3) is transformed into:

$$\eta''(\theta) + \left(\frac{G}{2\pi}\right)^2\left\{\mu^{2N}\eta(\theta) + \sum_{n=1}^{2N+1}\frac{a_n}{\left(a_{2N+1}\right)^{\frac{n-1}{2N}}}\mu^{2N+1-n}\eta(\theta)^n\right\} = 0\,. \tag{25}$$

Similarly, Eq. (5) is transformed into:

$$\eta''(\theta)+\left(\frac{G}{2\pi}\right)^2\left\{\mu^{2N}\eta(\theta)+\eta(\theta)^{2N+1}\right\}=0 \quad , \tag{26}$$

which, in the infinite-amplitude limit ($\mu \to 0$), becomes

$$\eta_0''(\theta)+\left(\frac{G_0}{2\pi}\right)^2\eta_0(\theta)^{2N+1}=0 \ . \tag{27}$$

In the large-N limit, $\eta_0(\theta)$ of Eq. (27) develops boundary-layer characteristics. The second term in Eq. (27) is exceedingly small, except near the turning points, where $\eta_0(\theta) = \pm 1$. Hence, over most of the range in θ, Eq. (27) generates for $\eta_0(\theta)$ a linear profile, the slope being $\pm v_{max}$. Only in the vicinity of the turning points ($\theta = 0, \pi, 2\pi, \ldots$) is this linearity replaced by a curved behavior, which ensures that $|\eta_0(\theta)|$ does not exceed 1. Considering the turning point at $\theta = 0$, the range in θ, over which $\eta_0(\theta)$ is curved, can be estimated. Taking into account that $\eta_0'(0) = 0$, approximating the (inner) solution near $\theta = 0$ by

$$\eta_0(\theta)=1-a\theta^2 \ , \tag{28}$$

and expanding Eq. (27) through $O(\theta^2)$, one finds

$$\eta_0(\theta)\approx 1-2(1+N)\frac{G_0^{\ 2}}{\pi^2}\theta^2 \ . \tag{29}$$

Matching of the solutions by requiring that $\eta_0'(\theta)$ (using Eqs. (29) reaches $(-v_{max})$ (see Eq. (23)) one obtains:

$$\theta_{matching}=\frac{\pi}{2G_0(N+1)}\left(1+O\left(\frac{1}{N}\right)\right)\underset{N\gg 1}{\cong}\frac{\pi}{2N}=\frac{1.5708}{N} \ . \tag{30}$$

A detailed numerical analysis reveals that the constant in large-N expression for $\theta_{matching}$ is close to 2.

Thus, as the power, $(2N + 1)$, grows, the range in θ, over which $\eta_0(\theta)$ deviates from the linear behavior diminishes. In summary, $\eta_0(\theta)$ is almost linear in θ. It bends nonlinearly to ± 1 close to the turning points. As a result, the profile of $\eta_0'(\theta)$ is almost constant at $\pm v_{max}$, and changes sign over a short range in θ around the turning points. Namely, as N grows, $\eta_0'(\theta)$ approaches a periodic step function. This is demonstrated in Fig. 2. $\eta_0(\theta)$ approaches a peri-

odic saw-tooth shape with linear segments, demonstrated in Fig. 3. Finally, thanks to the θ dependence of $\eta_0(\theta)$ and $\eta_0'(\theta)$, the phase-space plot of $\eta_0(\theta)$ vs. $\eta_0'(\theta)$ approaches a rectangle as N is increased, demonstrated in Fig. 4.

4. Large but finite x_{max}

4.1 General N

The zero-order approximation to $\eta(\theta)$, the solution of Eq. (25), when the latter is expanded in a power series in μ, is $\eta_0(\theta)$, the solution of Eq. (27). It is the infinite-amplitude limit of $\eta(\theta)$.

Consider the expansion of Eq. (25) in powers of μ^2. The next-to-highest-leading term in the expansion arises from two sources, both depending on what the next-to-highest leading term in Eq. (25) is. If lower-power terms, with $k = \{N-1,\ldots (N-q-1)\}$, are missing in Eqs. (3), so that the next-to-highest-leading term is $\eta(\theta)^{2q+1}$, $1 \le q \le N-1$, then the first correction in the curly brackets in Eq. (25) will be $O(\mu^{2(N-q)})$. In particular, in case of Eq. (5) the first correction term is of $O(\mu^{2N})$. Hence, for large but finite x_{max} the deviation of the full solution, $\eta(\theta)$, from the asymptotic solution, $\eta_0(\theta)$, becomes progressively smaller as N is increased.

4.2 The Duffing equation: Perturbation expansion for large but finite x_{max}

The Duffing equation offers an exception. In the large-amplitude limit, both the term in Eq. (13), which is linear in $\eta(\theta)$ and the period, T, add $O(\mu^2)$ terms to the expansion of Eq. (19) in powers of μ. Hence, as an example, the perturbation analysis of this case is presented here. The expansion of Eq. (19) yields:

$$\eta''(\theta)+\frac{8}{\pi}\left(\frac{\Gamma(5/4)}{\Gamma(3/4)}\right)^2\eta(\theta)^3+\mu^2\left(\frac{8}{\pi}\left(\frac{\Gamma(5/4)}{\Gamma(3/4)}\right)^2\eta(\theta)+\frac{\left(\sqrt{2}\,\frac{\Gamma(1/4)^3}{\Gamma(-1/4)}-2\pi\right)}{\pi^2}\eta(\theta)^3\right) \quad (31)$$

Writing

$$\eta(\theta)=\eta_0(\theta)+\mu^2\eta_2(\theta)\,, \quad (32)$$

the zero-order equation is solved by $\eta_0(\theta)$ of Eq. (21). The equation for $\eta_2(\theta)$ is:

$$\eta_2''(\theta)+\frac{24}{\pi}\left(\frac{\Gamma(5/4)}{\Gamma(3/4)}\right)^2\eta_0(\theta)^2\eta_2(\theta)+\frac{8}{\pi}\left(\frac{\Gamma(5/4)}{\Gamma(3/4)}\right)^2\eta_0(\theta)+\left(\frac{\sqrt{2}}{\pi^2}\frac{\Gamma(1/4)^3}{\Gamma(-1/4)}-\frac{2}{\pi}\right)\eta_0(\theta)^3 \quad (33)$$

To show how good the approximation through $O(\mu^2)$ is, $\mu = 0.3$ has ben chosen. For this choice, at the turning point, the cubic term in the Duffing equation is about ten times greater than the linear term: $((\varepsilon\, x_{\max}{}^2) = 1/0.3^2)$. Eqs. (31) and (33) have been solved numerically for $\eta(\theta)$ and $\eta_2(\theta)$, respectively. The zero-order solution, $\eta_0(\theta)$, of Eq. (21), provides an excellent approximation to the full solution, $\eta(\theta)$. This is demonstrated in Fig. 5. In the case of $\eta'(\theta)$, there is a small discrepancy between the full solution and the zero-order approximation. The situation is remedied by the effect of the second-order contribution of $\eta_2'(\theta)$, as demonstrated in Fig. 6. In summary, the quality of the second-order approximation is excellent although the cubic term is greater than the linear term in the equation by no more than a factor of

$$\varepsilon\, x_{\max}{}^2 = 1/\mu^2 = 11.11 \ .$$

5. Concluding comments

A perturbation expansion procedure has been developed for the computation of the solution of a nonlinearly perturbed harmonic oscillator in the limits of a large-amplitude and of a large power, $(2N+1)$, of the leading nonlinear monomial. This has been achieved through scaling of the oscillating variable and of time. The quality of the approximation to the full solution for the scaled variable, $\eta(\theta)$, is excellent even with the lowest-order term in the expansion.

The large-amplitude and large N limit of the solution, $\eta(\theta)$, exhibits boundary-layer characteristics. $\eta(\theta)$ may be viewed as the matching of an "outer" solution, which is linear in the scaled time variable, θ, and an "inner" solution, that reaches ± 1 at the turning points. Similarly, $\eta'(\theta)$ may be viewed as the matching of an "outer" solution, of a constant value, and an "inner" solution that reaches 0 at the turning points. As N grows, the range in θ near the turning points of the oscillations, where the "inner" solution evolves, shrinks as $O(1/N)$. The limiting shape for $\eta(\theta)$ is a periodic saw-tooth graph comprised of linear segments, for $\eta'(\theta)$ – a periodic step function and for the $\eta(\theta)$-$\eta'(\theta)$ phase plot – a rectangle.

Statements and Declarations

The author declares that no funds, grants, or other support were received during the preparation of this manuscript.

The author has no relevant financial or non-financial interests to disclose.

1) The author made all contributions to the conception or design of the work. No data acquisition was required. No new software was created.

2) The author drafted the work or revised it critically for important intellectual content;

3) The author approved the version to be published; and

4) The author agrees to be accountable for all aspects of the work in ensuring that questions related to the accuracy or integrity of any part of the work are appropriately investigated and resolved.

Data availability Statement

Data sharing is not applicable to this article, as no datasets were generated or analyzed during the current study.

References

1. R.E. Mickens, *Nonlinear Oscillations*, Cambridge University Press (1981).
2. A.I. Maimistov, Optics & Spectroscopy, **94**,251-257 (2003).
3. R.H. Rand, Lecture notes on nonlinear vibrations, Cornell University, pp. 13-17 (2012).
4. A. Elías-Zúniga, Appl. Math. Modelling, **37**, 2574-2579.
5. A. Beléndez et al., Nonlin. Dyn. **86**,1687-1700 (2016).
6. A. Beléndez et al., Adv. Math. Phys., **2017**, ID 7396063 (2017).
7. B.S. Wu and C.W. Lim, Int'l J. Nonlin. Mech., **39**, 859-870 (2004).
8. B.S. Wu, W.P. Sun and C.W. Lim, Int'l J. Nonlin. Mech., **41**, 766-774 (2006).
9. J.H. He, Chaos, Solitons and Fractals, **34**, 1430-1439 (2007).
10. L. Cveticanin, Int'l J. Nonlin. Sci. & Num. Simulat., **10**, 1491-1516 (2009).
11. D. Younesian, Computers & Math. Appl., **59**, 3222-3228 (2010).
12. M. Akbarzade and D.D. Ganji, Adv. Theor. Appl. Mech., **3**, 329-337 (2010).
13. S.K. Lai, C.W. Lim, Z. Lin and W. Zhang, Appl. Math. & Comp., **2017**,6115-6124 (2011)
14. S. S. Ganji, A. Barari, H. Babazadeh, M. G. Sfahani and G. Domairry, J. VibroEng., **13**, 219-231, (2011).
15. Y. Qian, D. Ren, S. Chen and L. Ping, Modern Mech. Eng., **2**, 167-165 (2012).
16. M. Akbarzade and Y. Kahn, Math. & Comp. Modelling, **55**, 480-489 (2012).
17. S. Durmaz and M.O. Kaya, J. Appl. Math., **2012**, ID 518684 (2012).
18. A. Beléndez et al., J. Appl. Math., **2012**, ID 286290 (2012).
19. S. Nourazar and A. Mirzabeigy, Scien. Iranica, **B20**, 364-368 (2013).
20. A. Nikkar, S. Bagheri and M. Saravi, Lat. Amer. J. Solids & Structures, **11**, 320-329 (2014).
21. S.R. Panigrahi, B. Feeny and A.R. Diaz, Proc. ASME 2014 Int'l Design Eng. Tech. Conf. & Conf. Mech. Vibrations & Noise, IDTEC/VIB 2014, DETC2014-34264, (August 17-20, 2014, Buffalo, NY, USA).
22. M. Kalami Yazdi and P. Hosseini Tehrani, Nonlin. Eng., **5**, 87-92 (2016)
23. A. Okasha El-Nady and M.M. A. Lashin, J. Mech. Eng. &Automation, **65**, 1100-116 (2016).
24. H.U. Molla, A. Razzak and M.S. Alam, Results in Physics, **6**, 238-242 (2016).
25. A.M. El-Naggar and G.M. Ismail, Alexandria Eng. J., **55**, 1581-1585 (2016).
26. J.H. He, Int'l J. Appl. Comput. Math. **3**, 1557-1560 (2017).
27. M.M Fatikh Karahan and M. Pakdemirli, Z. Naturforsch. **72a**, 59-69 (2017).

28. M.G. Sobamowo and A.A. Yinsua, J. Comput. Appl. Mech., **B48**, 297-306 (2017).
29. O. Gonzáles-Gaxiola, Int'l J. Appl. Comput. Math. **3**, 1249-1259 (2017).
30. M.S.H. Chowdhury, Results in Physics, **7**, 3962-3967 (2017).
31. G.M. Ismail, J. Egypt. Math. Soc.**25**, 434-437 (2017).
32. A. Big-Alabo, Mech. Eng. Res., **8**, 41-52 (2018).
33. R.K. Mahabadi an M.A. Pazhooh, Lat. Amer. J. Solids & Structures, **15**, e31 (2018).
34. N. Qie, W.F Houa and J.H He, Rep, Mech. Eng., **2**, 1-5 (2020).
35. G.M Ismail et al., J. Low Frequency, Noise & Active Control, **0**, 1-7 (2021).
36. L.A. MacColl, Am. J. Phys., **25**,535 (1957).
37. I.S. Gradshteyn and I.M. Ryzhik, *Tables of Integrals, Series and Products*, 7th edition, Elsevier (2007).

Figure Captions

Fig. 1 Large-amplitude limit G_0 (Eq. (7)) (red); Large-amplitude and large-N limit of G_0 (Eq. (8)) (blue).

Fig. 2 $\eta_0'(\theta)$ (Eq. (27)) vs. θ. $(2N+1) = 3$ (red), 5 (blue), 7 (green), 9 (brown), 21 (light blue), ∞ (black). Dashed – v_{max} (Eq. (23)).

Fig. 3 $\eta_0(\theta)$ (Eq. (27)) vs. θ. $(2N+1) = 3$ (red), 5 (blue), 7 (green), 9 (brown), 21 (light blue), ∞ (black).

Fig. 4 η_0 - η_0' phase-space plot (Eq. (27)). $(2N+1) = 3$ (red), 5 (blue), 7 (green), 9 (brown), 21 (light blue), ∞ (black).

Fig. 5 $\eta(\theta)$ (solution of Eq. (31), blue) and $\eta_0(\theta)$ (Eq. (21), red). $\mu = 0.3$.

Fig. 6 $\eta'(\theta)$ (solution of Eq. (31), blue) $\eta_0'(\theta)$ (Eq. (21), red) and second-order correction (using solution of Eq. (33), green). $\mu = 0.3$.

Figures

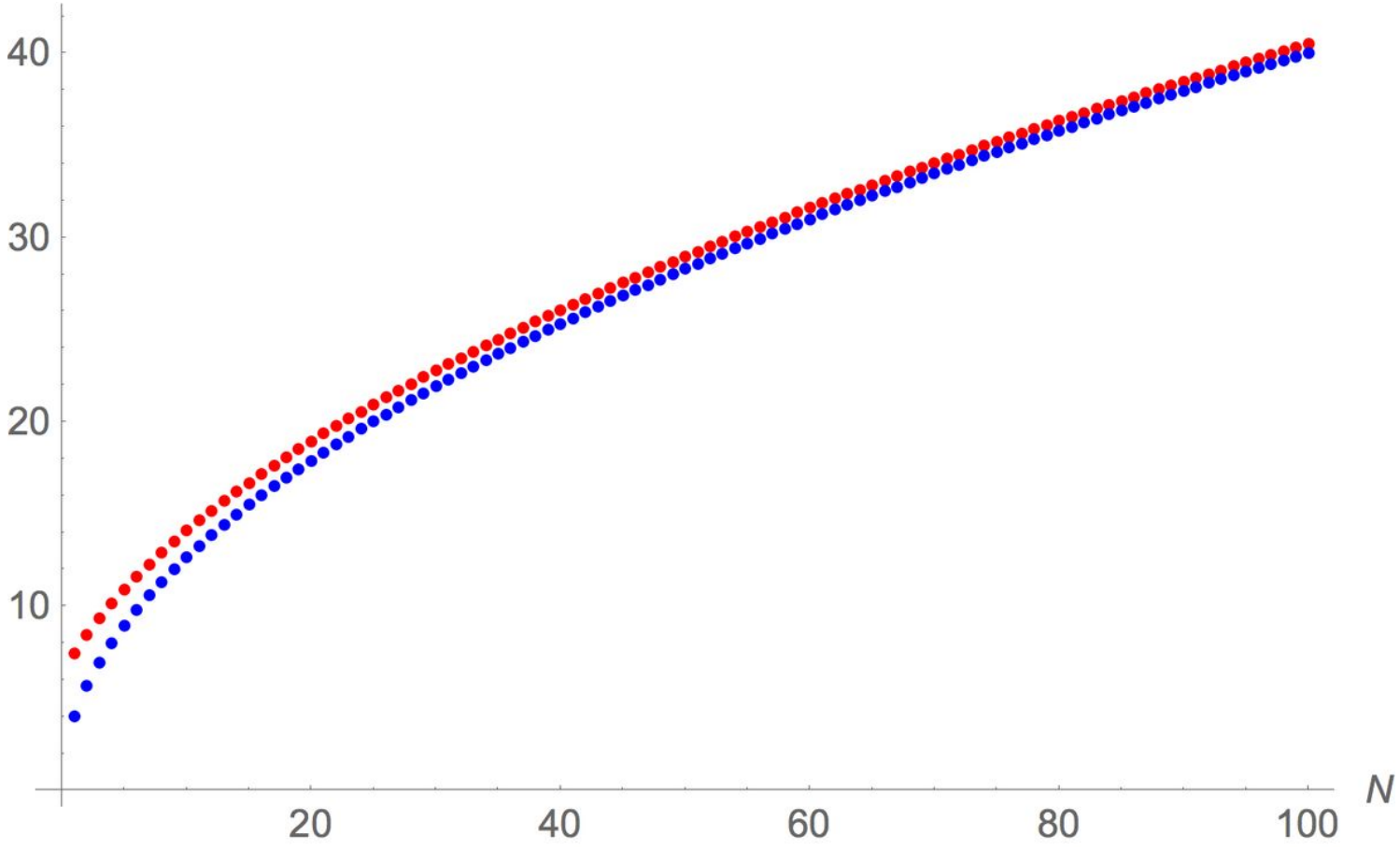

Figure 1

Large-amplitude limit G_0 (Eq. (7)) (red); Large-amplitude and large-N limit of G_0 (Eq. (8)) (blue).

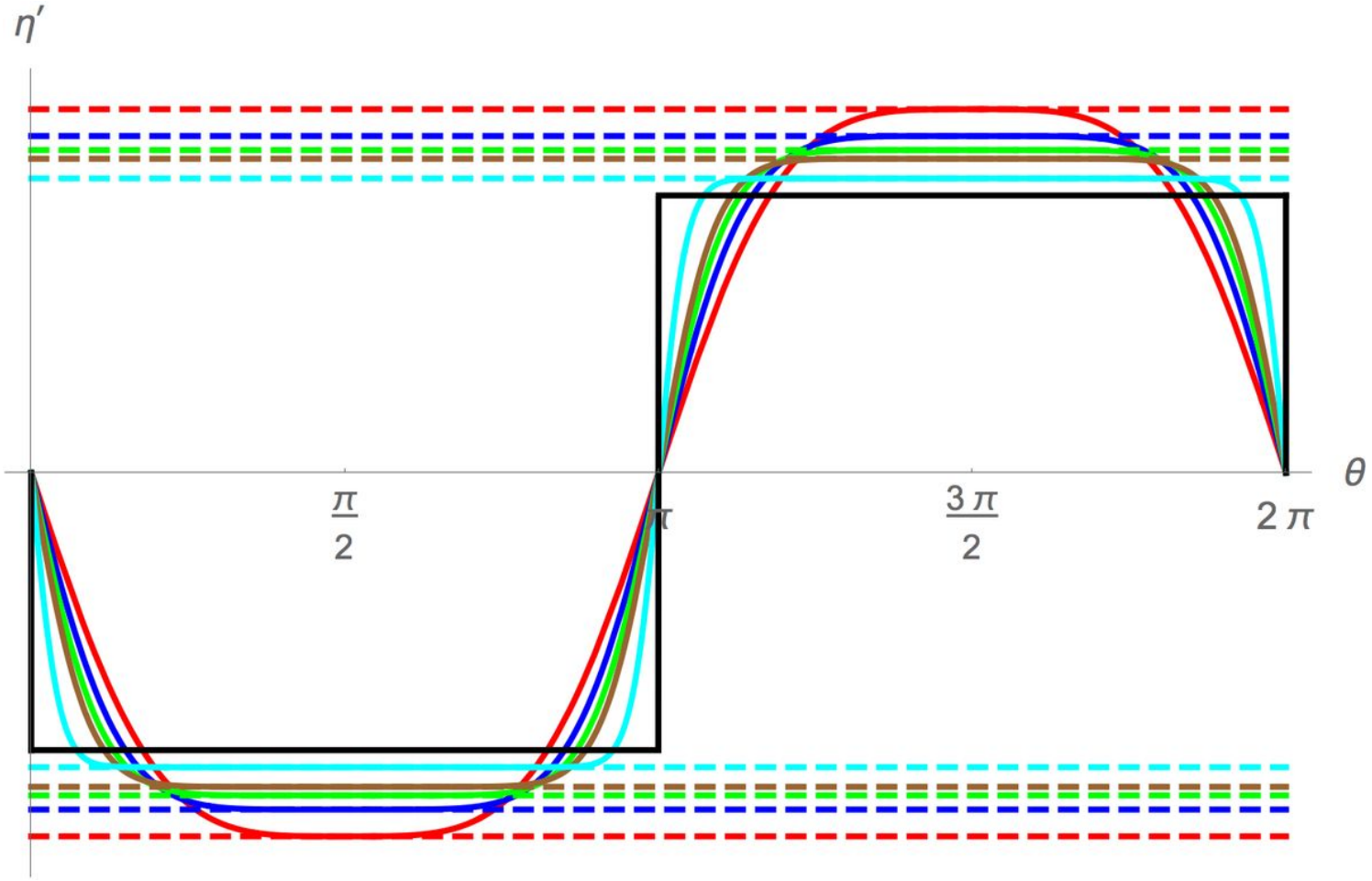

Figure 2

$\eta_0'(\theta)$ (Eq. (27)) vs. θ. (2 *N*+1) = 3 (red), 5 (blue), 7 (green), 9 (brown), 21 (light blue), ∞ (black). Dashed – v_{max} (Eq. (23)).

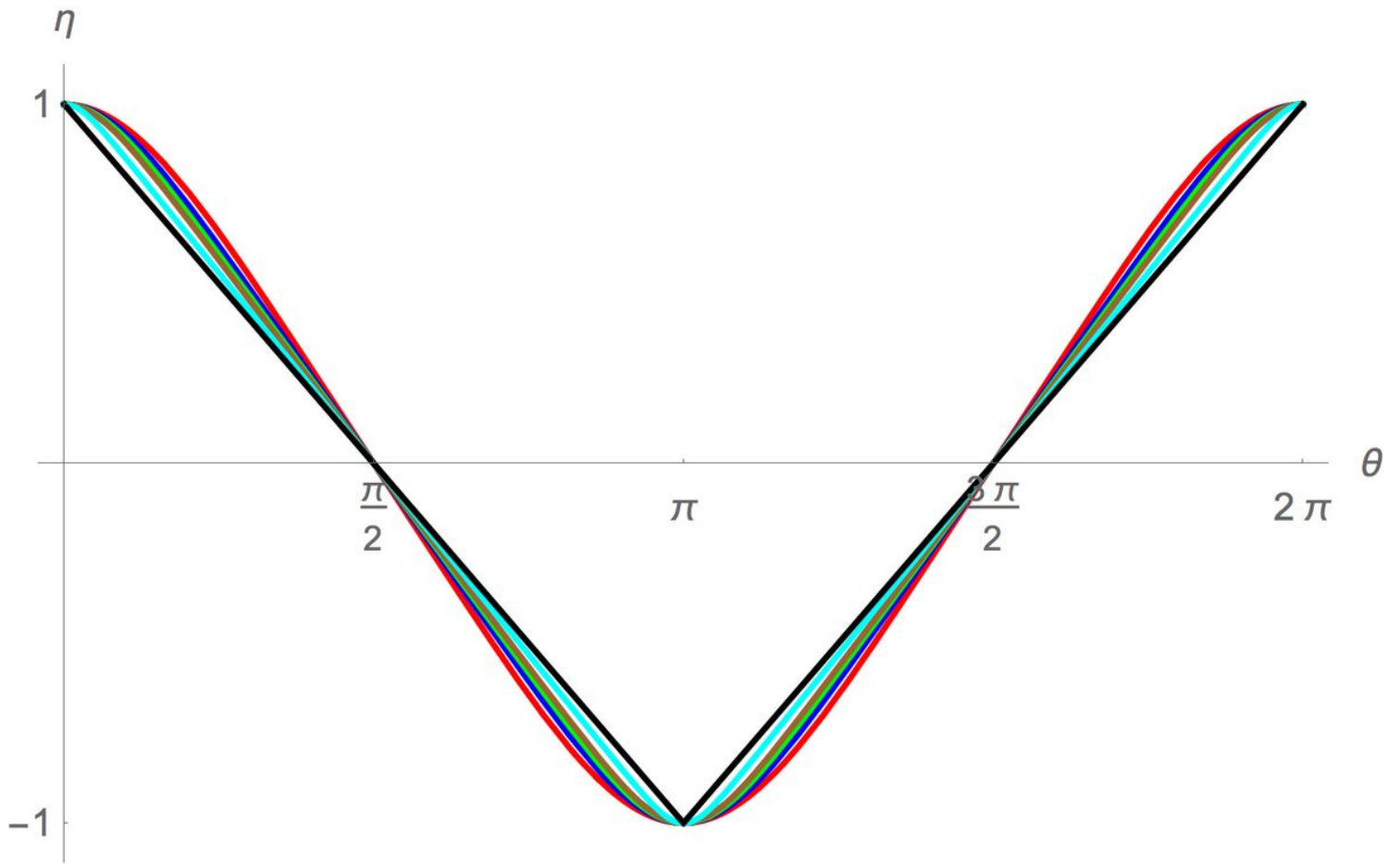

Figure 3

$\eta_0(\theta)$ (Eq. (27)) vs. θ. $(2\mathcal{N}+1) = 3$ (red), 5 (blue), 7 (green), 9 (brown), 21 (light blue), ∞ (black).

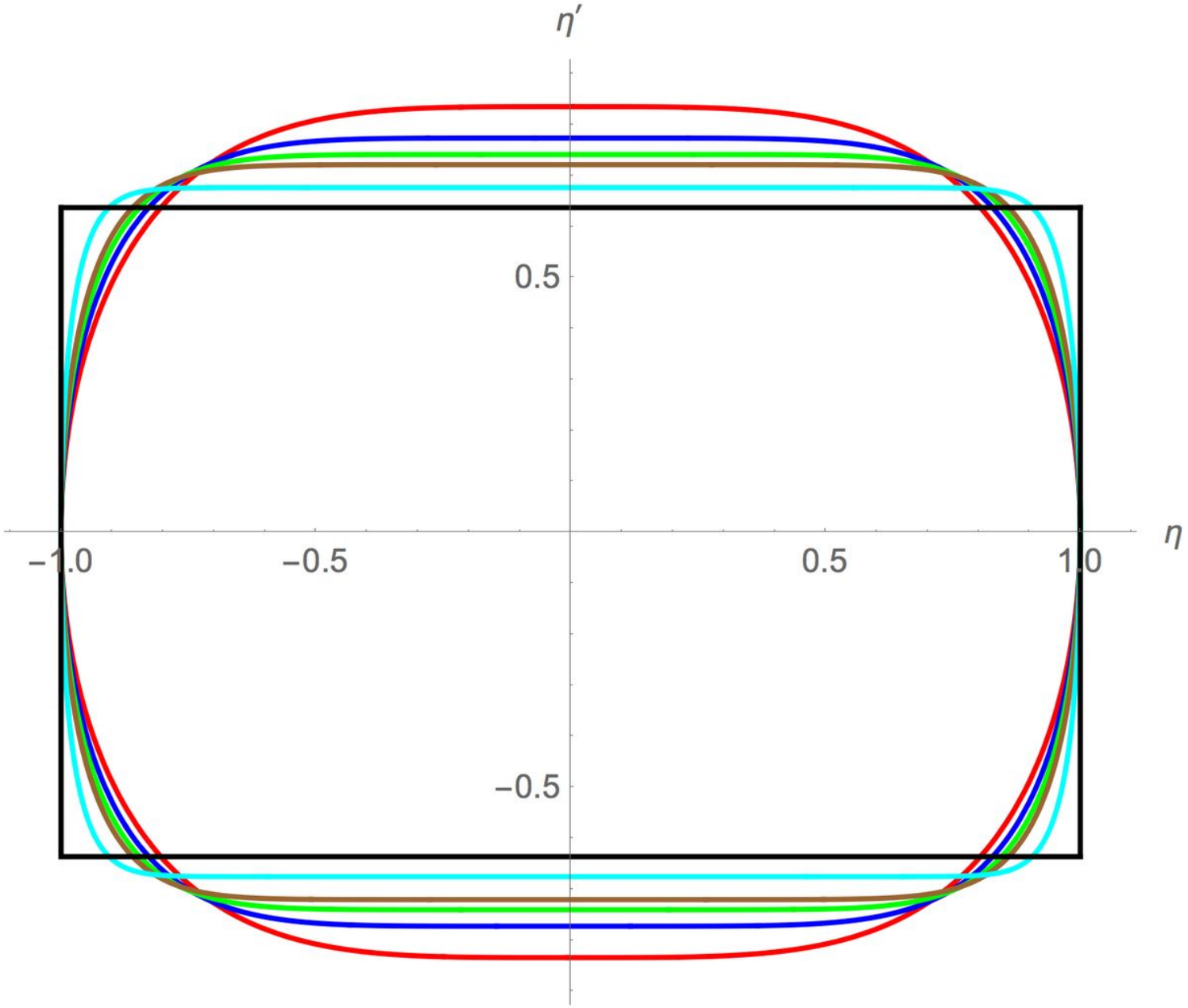

Figure 4

η_0 - η_0' phase-space plot (Eq. (27)). (2 N+1) = 3 (red), 5 (blue), 7 (green), 9 (brown), 21 (light blue), ∞ (black).

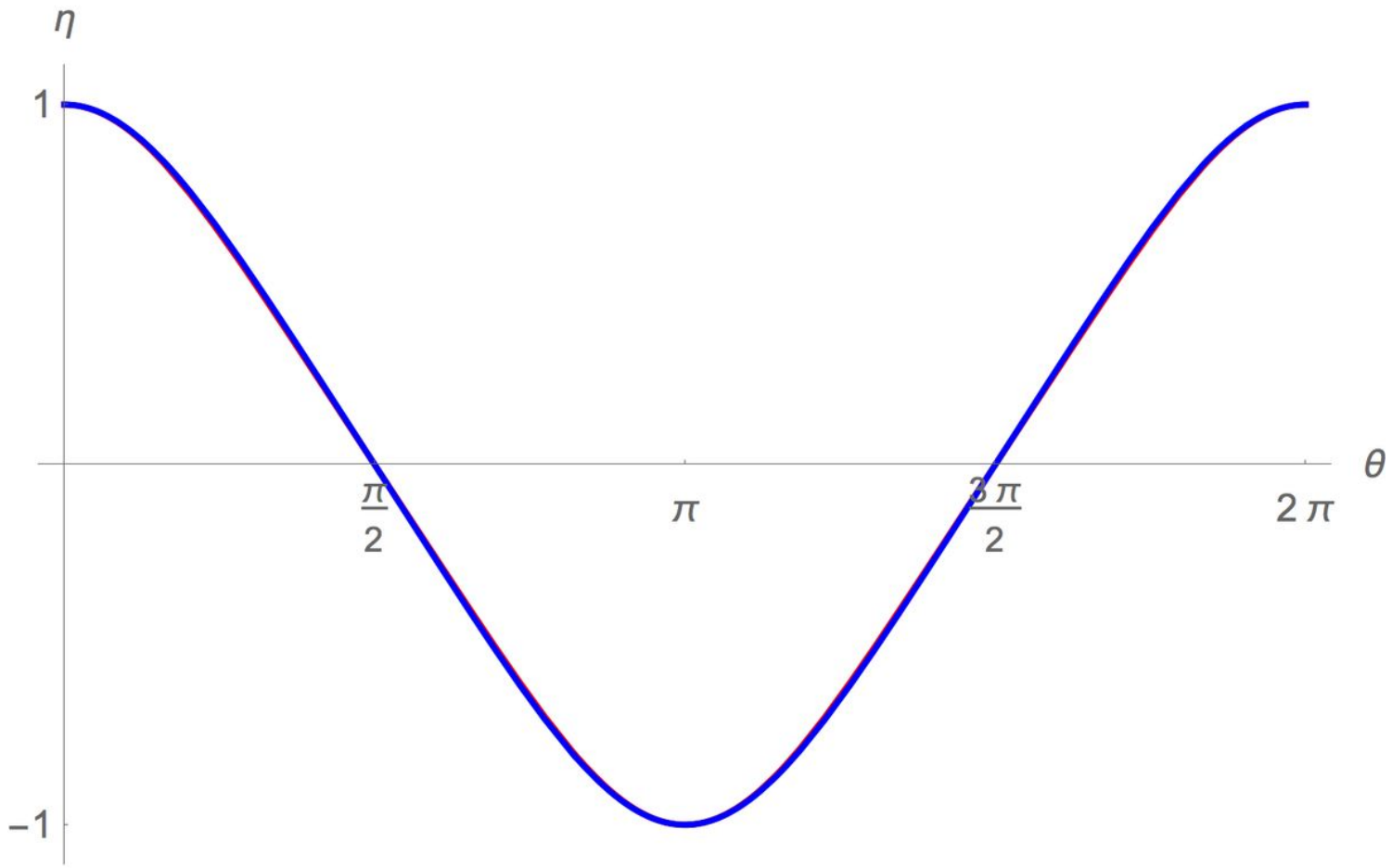

Figure 5

η(θ) (solution of Eq. (31), blue) and $\eta_0(\theta)$ (Eq. (21), red). μ = 0.3.

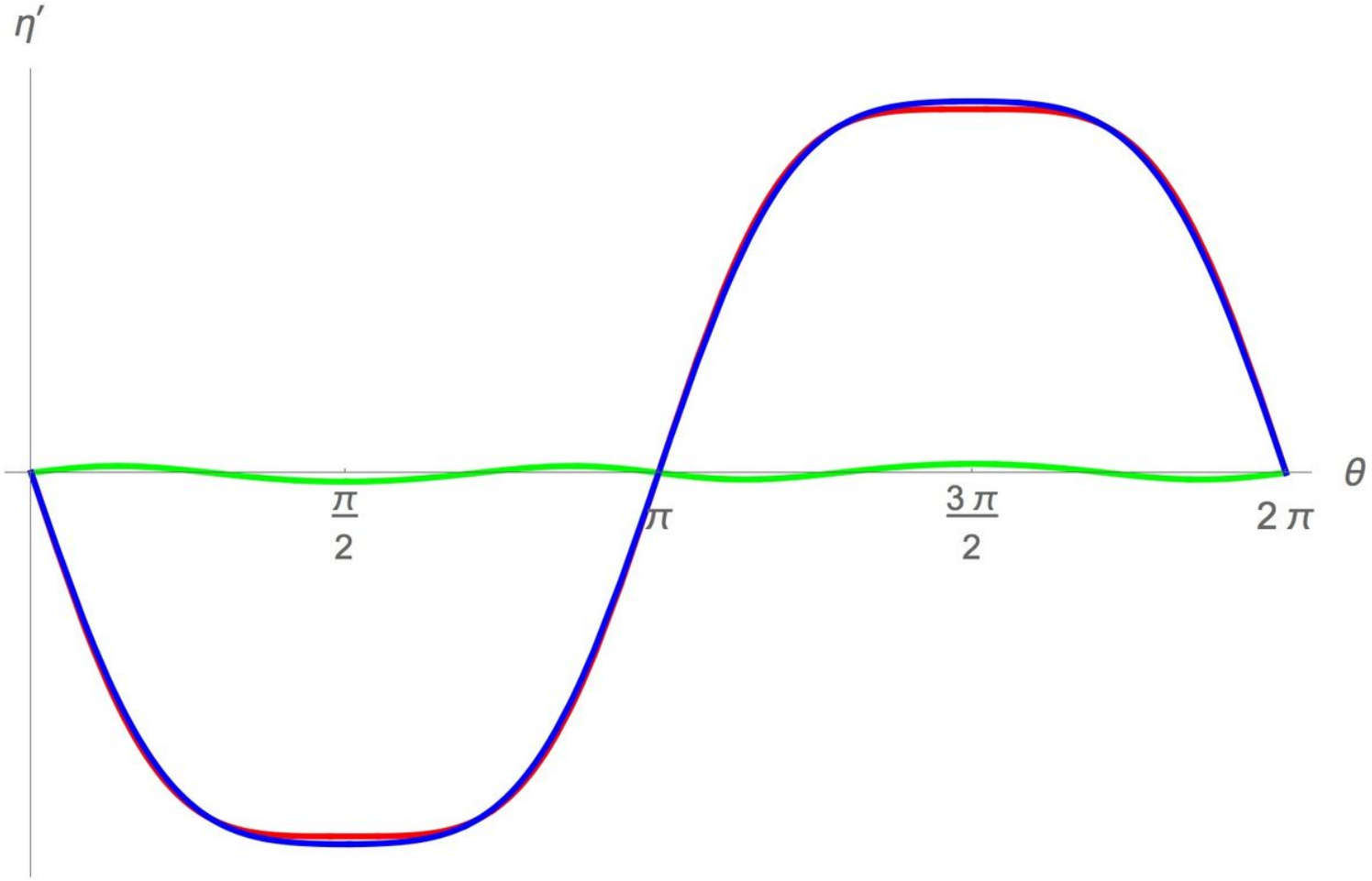

Figure 6

η'(θ) (solution of Eq. (31), blue) $\eta_0'(\theta)$ (Eq. (21), red) and second-order correction (using solution of Eq. (33), green). μ = 0.3.